J Appl Electrochem (2009) 39:1809–1819
DOI 10.1007/s10800-009-9884-4

ORIGINAL PAPER

Electrochemical evaluation of aminotriazole corrosion inhibitor under flow conditions

Armando Garnica-Rodriguez · J. Genesca · Juan Mendoza-Flores · Ruben Duran-Romero

Received: 2 October 2008 / Accepted: 29 March 2009 / Published online: 16 April 2009

Abstract The primary purpose of this study was to investigate the effect that turbulent pipe flow has on the electrochemical behaviour of a 3-amino-1,2,4-triazole (aminotriazole or 3-AT)-based corrosion inhibitor. The experiments were carried out in a 4-L laboratory pipe loop. A metallic ring made of API X52 pipeline steel was located in a linear segment of the pipe loop and acted as a test electrode. The test environment used in all experiments was a 3% NaCl solution saturated with CO_2 at 20 °C. The range of Reynolds number studied was from 6518 to 32118, assuring turbulent flow conditions in the pipe loop. Electrochemical impedance spectroscopy (EIS) was used to determine the electrochemical behavior of the steel in the environment at different flow rates and inhibitor concentrations. It was found that the electrochemical impedance of the system is dependent on both exposure time and flow conditions (Reynolds number). It was also detected that EIS data can give information on the persistence of the inhibitor film formed upon the metal surface. Therefore, in order to qualify the performance of the corrosion inhibitor, it is necessary to define the flow conditions at which it is intended to work.

Keywords Aminotriazole · Corrosion · CO_2 · Inhibitor · EIS · Flow

A. Garnica-Rodriguez · J. Genesca (✉)
Departamento de Ingenieria Metalurgica, Facultad Quimica, Universidad Nacional Autonoma Mexico (UNAM), Ciudad Universitaria, 04510 Mexico, DF, Mexico
e-mail: genesca@unam.mx

J. Mendoza-Flores · R. Duran-Romero
Direccion de Exploracion y Produccion, Corrosion, Instituto Mexicano del Petroleo (IMP), Eje Central Lazaro Cardenas # 1520, Mexico, DF, Mexico

List of symbols

R_{pif}	The resistance of the porous inhibitor film
ρ	The solution resistivity in the pores of the inhibitor films
d	The thickness of the inhibitor films
C_{pif}	The capacitance of the porous inhibitor film
C_s	The capacitance of solution in the pore
C_{inh}	The capacitance of inhibitor molecules
A_{pif}	The area occupied by the inhibitor film
A_{po}	The area of pores in the inhibitor film
A	The surface area of the EIS working electrode
ε_0	The electrical permittivity in vacuum (8.854×10^{-12} F m^{-1})
ε_{rf}	The relative electrical permittivity of the inhibitor film
ε_{rs}	The relative electrical permittivity of the electrolyte in porous inhibitor film

1 Introduction

In oil and gas production industry, internal corrosion of carbon steel pipeline is a well-known problem, and inhibition is the most effective and flexible method of corrosion control. Therefore, the knowledge of the mechanisms of the corrosion inhibition process is highly desirable in the design and proper selection of inhibitors.

In the petroleum industry, organic inhibitors containing nitrogen (amines) are often used due to their effectiveness and availability. When a corrosion inhibitor is added to a system, adsorption of inhibitor molecules occurs at the metal–solution interface. This adsorption is accompanied by a change in potential difference between the metal electrode and the solution, due to the non-uniform distribution of electric charges at the interface [1].

The use of film-forming inhibitors has been a widely used practice in the control of corrosion in hydrocarbon transport pipelines. The performance of these types of inhibitors depends on their ability to form a continuous film upon the surface of the metal that will be protected against corrosion, isolating it from the aggressive environment. In most cases, the corrosion environment is in constant movement. This is a common situation in the transport of hydrocarbons in steel pipelines. In industrial processes, fluid flow in pipes is usually turbulent. In order to obtain information about the performance of film-forming inhibitors, laboratory tests are carried out. The most common type of laboratory tests is based on weight loss of metallic coupons, which have been exposed to a test environment for a certain period of time. Some other tests use electrochemical measurements such as linear polarization resistance (LPR) or electrochemical impedance spectroscopy (EIS) to measure and monitor the rate of general corrosion. At the same time, it is known that, with limited success, the electrochemical techniques can be used for measuring the corrosion rate controlled by the diffusion of species in the flowing solution, i.e., flow-dependent corrosion rate. The thorough understanding of how these electrochemical techniques can be applied to a diffusion-controlled corrosion process occurring in flowing liquids and choosing the range of process parameters where the techniques can produce representative data are crucial for further improvement of the quality of experimental data obtained.

Some methodologies have been developed to assess the performance of film-forming inhibitors in moving environments. These methodologies use hydrodynamic test systems, such as rotating cylinders, impingement jets, or pipe loops. Pipe loops tend to be the widely used test systems, due to their geometrical similarity to actual pipelines and the availability of many mathematical descriptions. However, pipe loops can be very difficult to operate due to their large size, large amounts of chemicals and liquid environment used, requirements of pumping devices, and measurement equipments. This study explores the use of a pipe-loop system, one that can be easily operated and cleaned, to obtain valuable electrochemical data on the performance of a film-forming inhibitor under turbulent flow conditions, allowing the evaluation of corrosion inhibitors for the oil and gas industry.

The inhibitor-free CO_2 corrosion system selected has been previously investigated in the 1980s, and the results have been published in NACE books on CO_2 corrosion [2, 3]. Real corrosion rates were given while in the present publication only polarization resistance data from short-time electrochemical measurements are reported. The protectivity of carbonate scales changes with time, specifically in the first 48 h, and this was not taken into account.

2 Experimental procedure

A pipe loop was constructed with the following elements:

- One 1/12 HP magnetic pump, specially designed for corrosive fluids
- One variable resistance (rheostat) used to control fluid velocity in the loop
- PVC pipe segments of 1.27 cm of nominal diameter
- One 5 L conditioning plastic tank

The total volume of the pipe loop was 4 L.

The flow range used was from 0.0651 to 0.3210 L s^{-1}. This flow range corresponds to a Reynolds number, Re, range from 6518 to 32118. The flow loop was designed to achieve turbulent flow at the working electrode. The loop is capable of maintaining fluid flow values of up to 2.53 m s^{-1} operating at room temperature.

The flow loop was built with PVC tubes with an internal diameter of 1.27 cm, and the total length of the loop was 1.5 m. The schematic layout of this low-pressure and low-temperature system is shown in Fig. 1. Before each experiment, the system was deaerated with CO_2 for 5 h until the concentration of dissolved oxygen in the solution was less than 1 ppb. Since temperature and CO_2 partial pressure were constant, a constant pH value of 5.3 was measured during experiments. The test segment in the flow-loop was a three-electrode electrochemical cell. The electrochemical test segment in the pipe loop, shown in Fig. 2, contained:

- One AISI-1018 steel ring with an internal diameter of 1.27 and 3 cm width. This steel ring acted as the working electrode. Before each test, the steel ring was polished with 600-grit emery paper, cleaned with deionised water, degreased with acetone, and kept in a desiccator until its use.

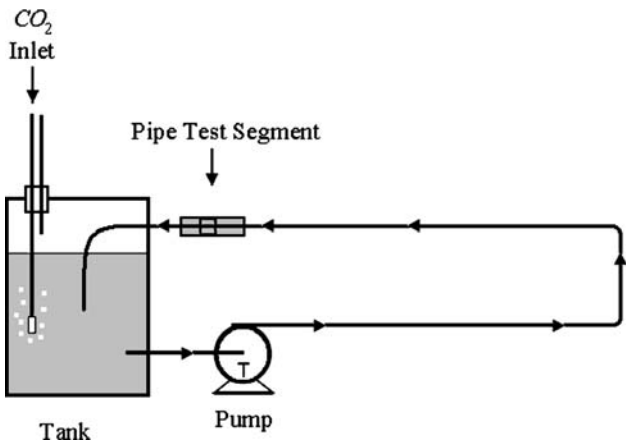

Fig. 1 Pipe flow loop diagram

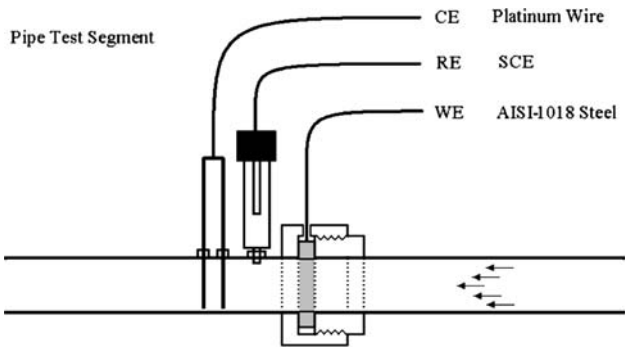

Fig. 2 Electrochemical pipe test segment (cross section) diagram: three-electrode set-up. *CE* counter electrode of platinum wire, *RE* reference electrode, saturated calomel electrode, *WE* working electrode, AISI-1018 steel ring

- One platinum wire. This wire was used as the counter electrode.
- One saturated calomel electrode (SCE) with a salt bridge, acting as the reference electrode.

Anodic and cathodic polarization tests and EIS measurements were carried out in this electrochemical test segment. The polarization tests were carried out to determine the effect of flow on the anodic and the cathodic kinetics of the corrosion process.

The test environment was an aqueous solution of 3% (weight) NaCl saturated with CO_2 gas (99.999% purity). All reactants used were analytically pure. The test solution was conditioned (pH, temperature, inhibitor concentration, and CO_2 bubbling) in the 5-L tank before it was pumped into the loop. The entire pipe loop was air-tight and the only gas purge was located at the conditioning tank.

The substance used as corrosion inhibitor was 3-amino-1,2,4-triazole, also known as aminotriazole or 3-AT, whose structure is shown in Fig. 3. This solid substance was previously dissolved in water in order to be easily added to the test environment. The inhibitor concentrations tested were 0, 25, 100, and 200 ppm. All electrochemical tests were carried out using a Solatron 1280B potentiostat controlled by a personal computer, running Scribner's Corrware software.

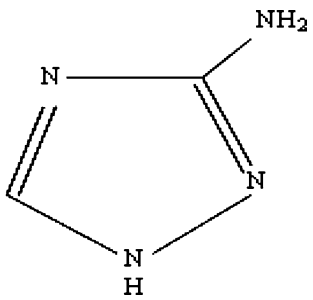

Fig. 3 Chemical structure of 3-amino-1,2,4-triazole (aminotriazole or 3-AT)

Polarization tests were carried out in the following conditions:

- CO_2 concentration = saturation
- Corrosion inhibitor concentrations: 0 ppm
- Temperature = 20 °C
- Atmospheric pressure
- Flow rates: 0.51, 0.70, 2.27, and 2.53 m s^{-1}

Electrochemical impedance spectroscopy (EIS) measurements were carried out at open-circuit potential (E_{corr}) with 10 mV AC voltage amplitude in the following conditions:

- CO_2 concentration = saturation
- Corrosion inhibitor concentrations: 0, 25, 100, and 200 ppm
- Temperature = 20 °C
- Atmospheric pressure
- Flow rates: 0.51, 0.70, 2.27, and 2.53 m s^{-1}

The experimental impedance results were analyzed in terms of equivalent circuits using ZView software. The equivalent circuit typically used to describe the behavior of film-formed inhibitor was used in this study.

All electrochemical tests were conducted once the steady-state was reached. The steady-state condition was considered achieved when the measured corrosion potential (E_{corr}) changed <5 mV during a 10 min period.

3 Experimental results and discussion

Polarization diagrams were used to determine Tafel regions, passivity, and regions under mass-transfer control.

3.1 Anodic polarization

Figure 4a shows two anodic polarization curves measured in the CO_2-saturated test solution, for full pipe flow at velocities of 0.51 and 2.53 m s^{-1}. These flow rates are the lowest and highest rates tested. It is observed that these anodic curves are identical; this fact indicates that there is no effect of flow on the anodic kinetics. This observation suggests that the anodic kinetics of the corrosion process is under activation control.

3.2 Cathodic polarization

Figure 4b shows four cathodic polarization curves measured in the CO_2-saturated test solution. These curves correspond to flow rates of 0.51, 0.70, 2.27, and 2.53 m s^{-1}. Here one notes that, at potentials lower than

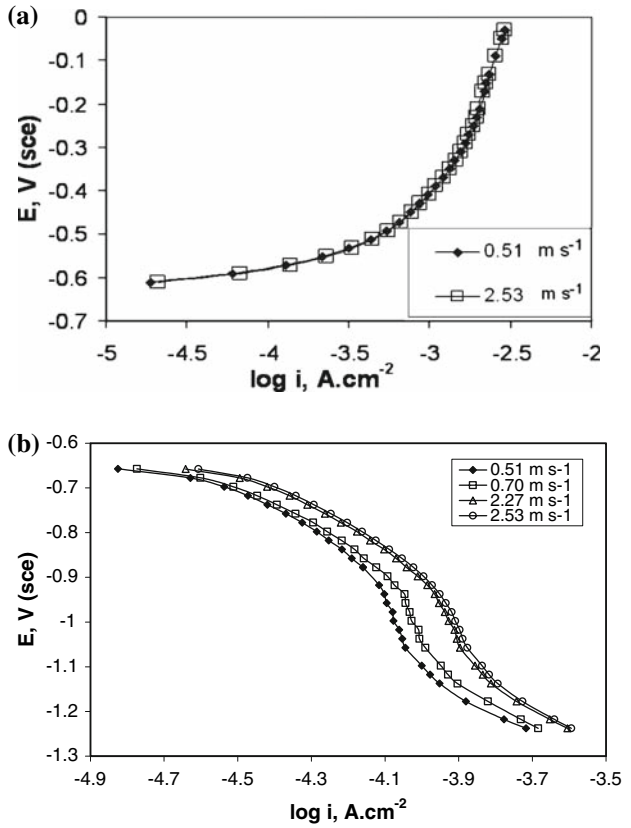

Fig. 4 AISI-1018 steel samples in pipe flow test segment, 3% (weight) NaCl aqueous solution, saturated with CO_2, 20 °C. **a** Anodic polarization curves at two flow rates. **b** Cathodic polarization curves at four flow rates

−0.95 V (SCE) approximately, the cathodic curves show a limiting current density (i_{lim}) section. This i_{lim} increases as the flow rate in the pipe segment also increases, from 4.37×10^{-4} A cm^{-2} at a flow rate of 0.51 m s^{-1} to 7.06×10^{-4} A cm^{-2} at a flow rate of 2.53 m s^{-1}. It is important to note that the increment of the measured i_{lim} between flow rates of 2.27 and 2.53 m s^{-1} is lower than the i_{lim} increment recorded between 0.51 and 2.27 m s^{-1}.

The effect of flow rate on the limiting current density is shown in Fig. 5. In order to determine if the cathodic process is under mass-transfer control, the values of limiting current densities, i_{lim} are taken from Fig. 4b at a potential value of −1.05 V (SCE) for each flow rate, within the mass-transfer region of the polarization curve. Plotting those i_{lim} values as a function of the flow rate, Fig. 5, a linear relationship can be observed. This analysis shows that the measured i_{lim} is affected by the flow rate and follows a linear behavior so that a mass-transfer control is expected.

The flow-dependent cathodic diffusion-limited current densities have been measured before in the 1970s [4] and explained in the literature [2, 3].

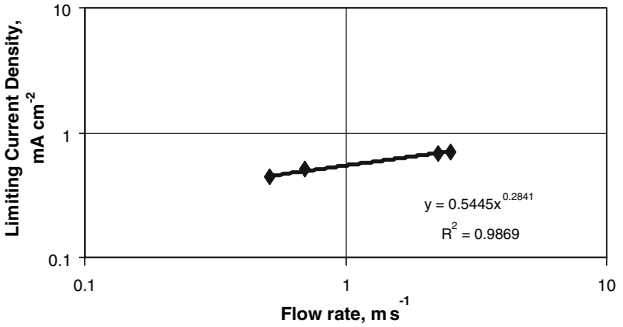

Fig. 5 Limiting current density, i_{lim}, as a function of flow rate

The electrochemical reaction that is assumed to be responsible for the cathodic process is

$$2H^+ + 2e^- \Rightarrow H_2. \quad (1)$$

Dissociation of H_2CO_3 serves as an additional source of H^+ ions, which are subsequently reduced according to Eq. 1.

In addition, there is a possibility that direct reduction of H_2CO_3 can take place:

$$2H_2CO_3 + 2e^- \rightarrow H_2 + 2HCO_3^-. \quad (2)$$

Reduction of bicarbonate ions and hydrogen evolution by direct reduction of water requires a pH > 5, and thus it is not taken into consideration.

Additionally, some important questions concerning the mass transport are not analyzed in this article, for example:

1. How is the mass transport occurring: through the pores? through the inhibitor?
2. What species are diffusing? Some candidates are: Cl^-, H_2O, H_2CO_3, CO_3^{2-}, and Fe^{2+}.
3. Is the thickness of inhibitor film mass transport controlled?

3.3 Corrosion potential, E_{corr}

E_{corr} measurements were made to detect the variations in the corrosion process taking place on the surface of the working electrode. As can be observed in Fig. 6a, the measured E_{corr} values slightly increased to the more noble (anodic) direction within the first few minutes of exposure.

Considering the flow rate (Re number), E_{corr} remains practically unchanged as the Re number increased. Figure 6b shows the measured values of E_{corr} versus the flow rate in terms of the Re number. This behavior is unexpected for a mass-transfer controlled process.

3.4 Effect of aminotriazole on E_{corr}

The effect of aminotriazole concentration on the E_{corr} is shown in Fig. 7. As can be observed, the change of

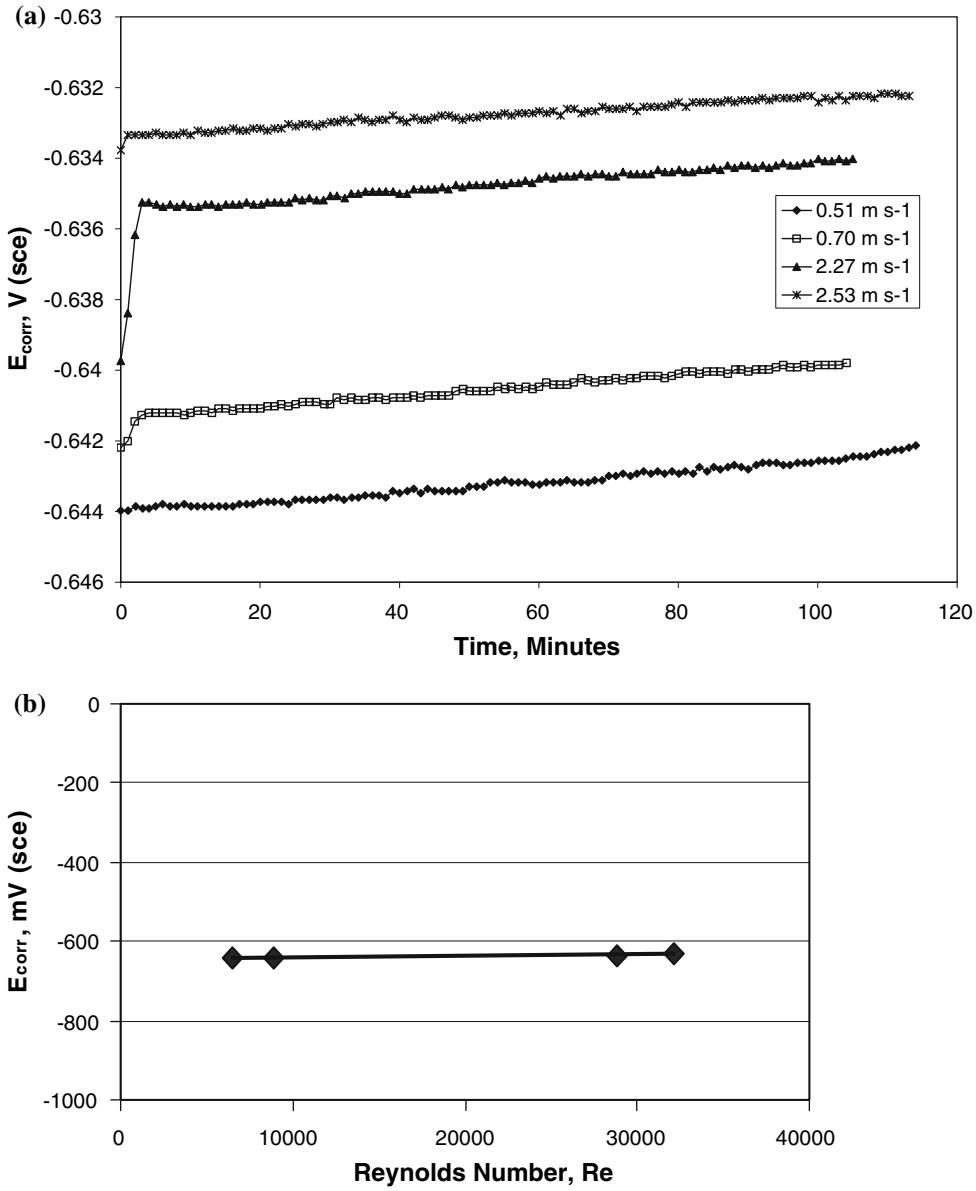

Fig. 6 **a** Corrosion potential, E_{corr} as a function of immersion time. **b** Corrosion potential, E_{corr}, as a function of Re number

corrosion potential E_{corr} due to the addition of aminotriazole is negligible. Previous studies [5, 6] show that, if the shift of corrosion potential due to the addition of an interface inhibitor is negligible, the inhibition is most probably caused by a geometric blocking effect of the adsorbed inhibitive species on the surface of the corroding metal. Therefore, a possible way to decrease the corrosion is the blocking of the active sites on the metal surface by adsorbed aminotriazole molecules. This may change the average activation energy barriers of the anodic and cathodic reactions, and thus change the corrosion potential. This happens because the adsorption of aminotriazole molecules is a chemical adsorption process, which involves the donation of a pair of electrons present on the nitrogen atom to iron metal. The N–C–N bond in aminotriazole molecules possess the p–π conjugation property, which remarkably strengthens the chemical adsorption of the nitrogen atom on the metal surface [7, 8].

When no inhibitor is present, a layer of corrosion product $FeCO_3$ mixed with Fe_3C is present on the metal surface [9]. This non-protective layer will form additional cathodic reaction sites, and thus will not decrease the overall corrosion rate. The non-conductive nature and cathodic properties of iron carbonate scales even in the presence of Fe_3C have been demonstrated by Schmitt et al. [10]. Therefore, the main function of the adsorption of aminotriazole molecules is to block these active sites and change the reaction activation energy.

Furthermore, the adsorbed aminotriazole molecules could also form an interface network above the metal surface, restraining the movement from the bulk solution to the metal surface of the corrosion product Fe^{2+} and the

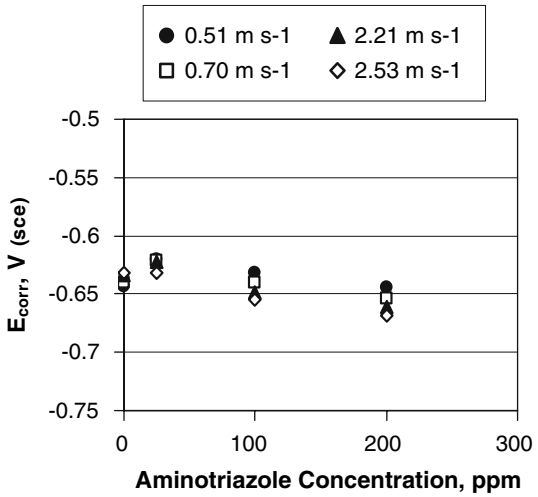

Fig. 7 Corrosion potential E_{corr} as a function of aminotriazole concentration at different flow rates

electrochemical active species H^+, HCO_3^-, and H_2CO_3. The accumulation of ferrous ion (Fe^{2+}) next to the metal surface will increase its local concentration in situ, increase supersaturation with respect to iron carbonate $FeCO_3$ at the surface, and lead to the formation of iron carbonate in the pores. This will reduce the number of active sites [9].

3.5 Electrochemical impedance spectroscopy (EIS)

Figure 8a–d show the EIS data measured at different flow rates and inhibitor concentrations as Nyquist diagrams. The equivalent circuit typically used to describe the behavior of an electrode coated with a non-conducting inhibitor film was used in this study [11–13]. This circuit is shown in Fig. 9. The shape of the impedance spectra and the nature of chemical compound used as inhibitor suggested that the impedance response of the system can be fitted by an equivalent circuit model that considers a coated metallic surface, a R(RC)(RC) circuit.

Figure 8a shows the Nyquist impedance plot of the carbon steel measured in the test solution at flow rates of 0.51, 0.70, 2.27, and 2.53 m s^{-1} and inhibitor concentration of 0 ppm (blank test). Figure 8a shows that the Nyquist impedance plots are semicircles at the four flow rates tested. This observation indicates that the same electrochemical process is taking place at all the flow rates tested. This means that the electrode reaction is controlled only by charge transfer. This behavior can be interpreted according to a simple circuit model, $R_s(R_{ct}C_{dl})$. The impedance associated with the solution resistance (R_s) is 24 Ω cm^2 R_{ct} is the metal charge-transfer resistance, and C_{dl} is the double layer capacitance. R_{ct}, which represents corrosion rate, can be obtained by the intersection of the diameter of the semicircle with the real impedance axis. In general, as the flow rate increases, the measured impedance decreases, that is, the diameter of the semicircle R_{ct}, decreases. The impedance values measured at the lower frequency values of the spectra that is associated with the charge-transfer resistance (R_{ct}) change from 213 Ω at a flow rate of 0.51 m s^{-1} to 149 Ω at a flow-rate of 2.53 m s^{-1} (Fig. 8a). By comparing R_{ct} at different velocities, it is found that at E_{corr} potential value, R_{ct} decreases with increase in velocity. This indicates that the corrosion rate becomes high as the velocity is increased.

Figure 8b shows the EIS data measured in the test solution at flow rates of 0.51, 0.70, 2.27, and 2.53 m s^{-1} and an inhibitor concentration of 25 ppm. The shape of the impedance spectra is similar to those shown in Fig. 8a. This observation indicates that the same electrochemical process is taking place at all the tested flow rates in the presence of inhibitor. The impedance associated with the solution resistance (R_s) is 26 Ω cm^2. The flow dependence of the impedance, shown in Fig. 8a, can also be observed in the presence of 25 ppm of inhibitor. However, there is no clear effect of the inhibitor on changing the diameter of the measured semicircles. This observation indicates that, at this concentration, the inhibitor has no effect on the electrochemical process.

Figure 8c shows the EIS results measured in the test solution at the four flow rates studied 0.51, 0.70, 2.27, and 2.53 m s^{-1} and an inhibitor concentration of 100 ppm. The shapes of the impedance spectra are similar to the ones observed at concentrations of 0 and 25 ppm of inhibitor in the test solution, indicating that the same electrochemical process takes place on the surface of the test coupons. There is also a clear flow dependence of the measured impedance. As the flow rates increase, the measured diameter of the semicircles recorded decreased. The measured R_{ct} value varies from 772 Ω at a flow-rate of 0.51 m s^{-1} to 155 Ω at a flow rate of 2.53 m s^{-1}. It is also evident that the impedance values are, in general, higher that those shown in Fig. 8a, b. This fact clearly indicates that there is an effect of this concentration of inhibitor upon the measured corrosion rate. It can be said that, at 100 ppm, the tested inhibitor decreases the corrosion rate of the steel. However, this inhibiting effect is affected by flow rate. As the flow rate increases, the corrosion rate is also increased.

Figure 8d shows the EIS results measured in the test solution at flow rates of 0.51, 0.70, 2.27, and 2.53 m s^{-1} and an inhibitor concentration of 200 ppm. The shapes of the EIS spectra are similar to those found in all previous Fig. 8a–c, indicating that the electrochemical process taking place is essentially the same at all conditions. In general, at this inhibitor concentration, the measured impedance showed the highest values of all experiments.

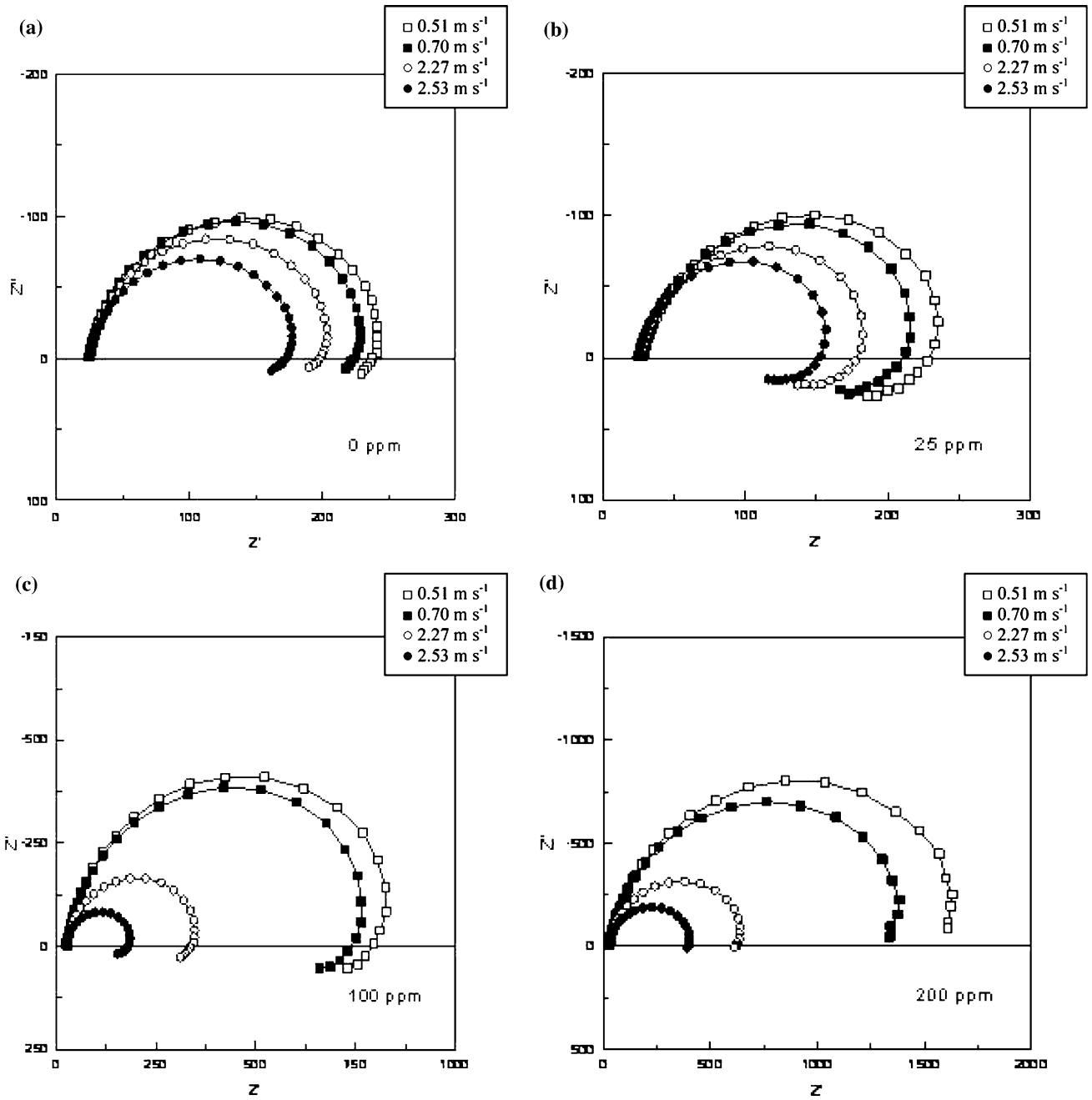

Fig. 8 Nyquist representation of the impedance at four flow rates. AISI-1018 steel samples in pipe flow test segment, 3% NaCl aqueous solution, saturated with CO_2. **a** No inhibitor added (0 ppm), 20 °C; **b** corrosion inhibitor concentration of 25 ppm, 20 °C; **c** corrosion inhibitor concentration of 100 ppm, 20 °C; and **d** Corrosion inhibitor concentration of 200 ppm, 20 °C

The associated values of R_{ct} measured vary from 1,584 Ω, at a flow rate of 0.51 m s^{-1}, up to 369 Ω, at a flow-rate of 2.53 m s^{-1}. This fact clearly indicates that the lowest corrosion rates can be expected at this inhibitor concentration at all flow rates tested. However, there is a clear flow dependency of the measured impedance. Therefore, the expected corrosion rate has a flow dependency. In general, as the flow rate increased the measured corrosion rate also increased.

Additionally, most of the EIS diagrams clearly exhibit an inductive loop in the low frequency range; such behavior is common in the case of CO_2 corrosion. This low frequency time constant is ignored for the moment in the analysis of impedance. Thus, the equivalent circuit proposed does not fit the low-frequency part of the Nyquist diagrams.

Considering the nature of the chemical compound used as inhibitor and recognizing that in the Nyquist representations of the EIS data well-defined semicircles are

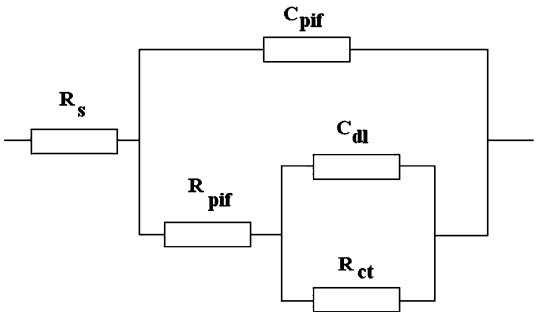

Fig. 9 Equivalent circuit used. R_s solution resistance, R_{ct} charge-transfer resistance, C_{dl} capacitance of the double layer, R_{pif} resistance in the porous inhibitor film, and C_{pif} capacitance in the porous inhibitor film

obtained, a R(RC)(RC) typical equivalent circuit was used, Fig. 9, to analyze the results. This circuit considers a solution resistance (R_s), a solution resistance in porous inhibitor film (R_{pif}), a capacitor inhibitor film (C_{pif}), a charge-transfer resistance (R_{ct}), and a double layer capacitance (C_{dl}). All the experimental data were fitted to this electric circuit model, using Scribner's Zplot software Version 2.7.

The slight increase of corrosion rate (represented as $1/R_{ct}$ values) without inhibitor, shown in Fig. 10a may suggest that little or no protective corrosion-product film has been formed on the metal surface. Little information has been reported concerning the electrochemical behavior of corrosion layers formed on steel in-pipe flow. When carbon steel is exposed, the corrosion product $FeCO_3$ and the iron carbide, cementite, Fe_3C from the steel itself may form a mixture on the metal surface [14]. The main effect of cementite is then to form additional cathodic reaction sites. The solubility of $FeCO_3$ is less sparingly soluble in a CO_2 containing solution with a high HCO_3^- content [15].

Therefore, it is possible that most of the product of anodic reaction, ferrous ion, will dissolve in the water-forming $FeCO_3$ scales especially at high turbulent conditions. This will then leave at the steel surface some uncorroded Fe_3C released from the corroded steel. This forms a conductive, porous layer on which the cathodic reaction can take place.

Figure 10a shows the corrosion rate, as $1/R_{ct}$, at different flow rates. It can be seen that the $1/R_{ct}$ at 200 ppm is lower than those at 100 and 25 ppm. This indicates that the inhibitor is more effective at this concentration under turbulent flow conditions, independent of the flow rate. This also suggest that the charge-transfer resistance from EIS tests could be used to study and compare the corrosion rates under different flow conditions. These results indicate that the corrosion process is impeded by the addition of the inhibitor.

Grimm and Landolt [15] explained that a mass-transport limited current plateau, such as can be seen in Fig. 4b, can

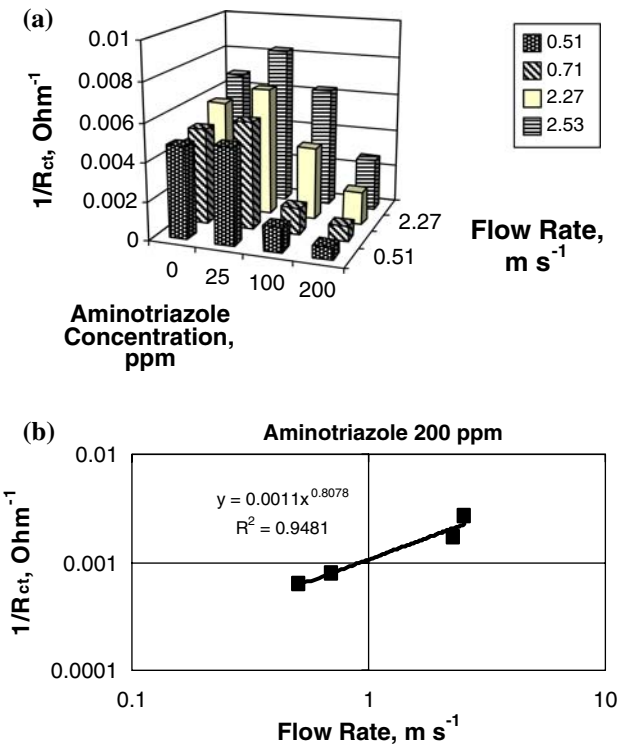

Fig. 10 **a** Calculated values of the charge-transfer resistance (R_{ct}), inverse values, as a function of aminotriazole concentration and flow rate in the pipe test segment and inhibitor concentration. **b** Corrosion rate, as $1/R_{ct}$, as a function of flow rate. Aminotriazole concentration: 200 ppm

be due to the formation of a corrosion product layer. They pointed out that the rate of dissolution at the current limit was controlled by the rate of mass transport of ferrous ion from the layer into the solution.

One useful method to characterize the mass-transfer influence on the corrosion process is the analysis proposed by Silverman [16], but it should be pointed out that this approach is valid for rotating cylinder electrodes.

Plotting the inverse of R_{ct}, $1/R_{ct}$, as a measure of the estimated corrosion rate versus the logarithm of the flow rate a linear relationship can be observed (Fig. 10b). If the data points or slope are similar to those expected from the literature-derived relationship for the rotating cylinder, mass transfer probably controls the corrosion rate. Performing a linear regression of the data points produces a reasonable agreement between measured and calculated values in the regression. This analysis provides experimental evidence that corrosion rate in turbulent flow conditions could be diffusion controlled. According to Silverman [16], if the slope of the regression, 0.81 in this particular case, Fig. 10b, corresponding to 200 ppm of aminotriazole is much greater than 0.75, artifacts such as surface roughness or particulate erosion could be affecting the results. If the slope of the regression lies between about

0.65 and 0.75, the corrosion rate is likely to be significantly influenced or even controlled by mass transfer.

Figure 10a shows the comparison of corrosion rate values as $1/R_{ct}$ at 0, 25, 100, and 200 ppm of inhibitor as a function of the flow rate. The most remarkable phenomenon in the diagram is that the $1/R_{ct}$ values at 200 ppm are very low. Further, the $1/R_{ct}$ values at 25, 100, and 200 ppm of inhibitor continuously increase as a function of flow rate, which suggest that the inhibitor is more effective at lower flow rates and provides experimental evidence about the weakness of the inhibitor film.

Many researchers have been working on the performance and mechanisms of the inhibitors based on the test results in small-scale laboratory systems. The studies of Mansfeld [17] point out that the interface inhibition presumes a strong interaction between the corroding substrate and the inhibitor. The two-dimensional adsorbate layer can affect the basic corrosion reactions in various ways [9]:

- that caused by the geometric blocking effect of adsorbed inhibitive species on the metal surface;
- that due to the effect of blocking the active sites on the metal surface by adsorbed inhibitive species;
- that due to the electrocatalytic effect of the inhibitor or its reaction products.

For the first case, the inhibition comes from the reduction of reaction area on the surface of the corroding metal, whereas for the other two models, the inhibition effects are due to the changes in the average activation energy barriers of the anodic and cathodic reactions of the corrosion process.

In this study, an equivalent circuit model shown in Fig. 9 is proposed to simulate the simple corrosion processes shown in Fig. 11. According to the previous sudy [18–21], the R_{pif} in Fig. 9 has been interpreted as the pore solution resistance due to electrolyte penetration through the pores of inhibitor film. The capacitance C_{pif} has been interpreted as the capacitance of the dielectric inhibitor film. However, in a real system, film on the metal surface is a complex layer of both inhibitor and corrosion products films [9]. In this study, the film on the metal surface when inhibitor is present in solution is simply treated as inhibitor film since inhibitor molecules also treat corrosion product layer as its surface. The resistance and capacitance of the porous film can be written as [9, 18, 20].

$$R_{pif} = \rho \frac{d}{A_{po}} \tag{3}$$

$$C_{pif} = C_s + C_{inh} = \varepsilon_0 \varepsilon_{rs} \frac{A_{po}}{d} + \varepsilon_0 \varepsilon_{rf} \frac{A_{pif}}{d} = \varepsilon_0 \varepsilon_{rs} \frac{A_{po}}{d} + \varepsilon_0 \varepsilon_{rf} \frac{A - A_{po}}{d} \tag{4}$$

Figure 12 shows the results obtained. As shown in this figure, the pore solution resistance R_{pif}, which represent the diffusivity of the electroactive species, decreases as a function of the flow rate, especially for the higher flow rate values. It is also obvious that higher R_{pif} values are obtained for 200 ppm of aminotriazole. By increasing inhibitor concentration, two effects can be expected: an increase of the thickness of the inhibitor film d and a decrease in the area of pores in the inhibitor film. Accordingly, an increase in R_{pif} values occurs.

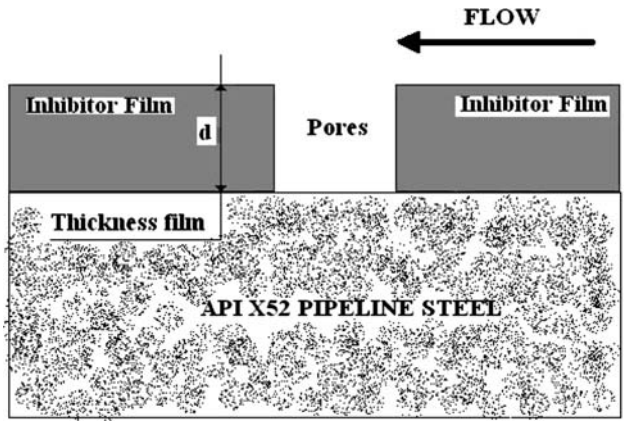

Fig. 11 Schematic of a simple inhibitor film model [9]

On the contrary, the effect of flow seems to affect the persistence of the inhibitor film formed upon the metal surface. The introduction of an inhibitor into the electric double layer changes its composition and structure [1]. The inhibitor molecules on the metal surface affect the electric double layer by causing a change in the dielectric properties of water molecules in the electric double layer. In this case, they may change the orientation of the dipoles of the water molecules which causes lowering of the dielectric constant and then decreases the double-layer capacitance. The decrease of double-layer capacitance may also be due

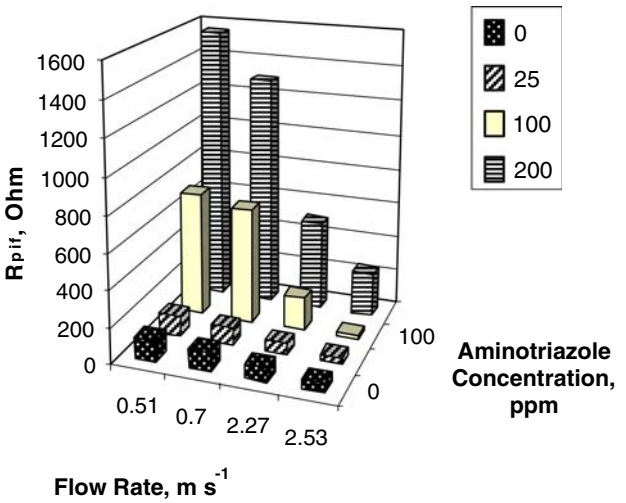

Fig. 12 Pore solution resistance due to electrolyte penetration through the pores of inhibitor film R_{pif} as a function of flow rate and aminotriazole concentration

to the decrease of the area where electrolyte is present due to the formation of the inhibitor film [9].

Equation 4 shows that the overall film capacitance is the combination of capacitance of inhibitor molecules and the solution capacitance in the pores. When more and more inhibitor molecules adsorb on the surface, it can be seen, Fig. 13, that the inhibitor film capacitance C_{pif} becomes much lower. The decrease of overall film capacitance may suggest that the electrical permittivity of inhibitor molecules is relatively much lower compared to the relative electrical permittivity of water, about 80 (20 °C). Therefore, the decrease of the capacitance could result from both the increase of area (A_{pif}) where inhibitor molecules adsorb and the increase of thickness (d) of the inhibitor film.

On the other hand, the R_{pif}, which represents the resistance of electrochemical species transporting to and from the surface and bulk solution, increases from 120 Ω at 25 ppm to 1,550 Ω at 200 ppm at the lower flow rate, 0.51 m s^{-1}, Fig. 12. Since the R_{pif} is proportional to the thickness of the path in which electrochemical species diffuse and C_{pif} is inversely proportional to the thickness of the film, the increase of the thickness of the inhibitor film is then unexpected. Thus, the decrease of the pore size due to the formation of a dense inhibitor film may explain the phenomenon. The reduction of the pore size decreases not only the overall diffusion area (A_{po}) but also the conductivity of the electrochemical species in the porous medium. A very dense inhibitor film will also decrease the number of the kinetic active sites where the anodic and cathodic reactions can take place, and, accordingly, decrease the corrosion rates [9].

From the above analysis, it can be concluded that the formation of a dense inhibitor film on the metal surface can be used to explain both the decrease of charge-transfer resistance and the decrease of the electrical properties such as the porous film inhibitor (C_{dl}).

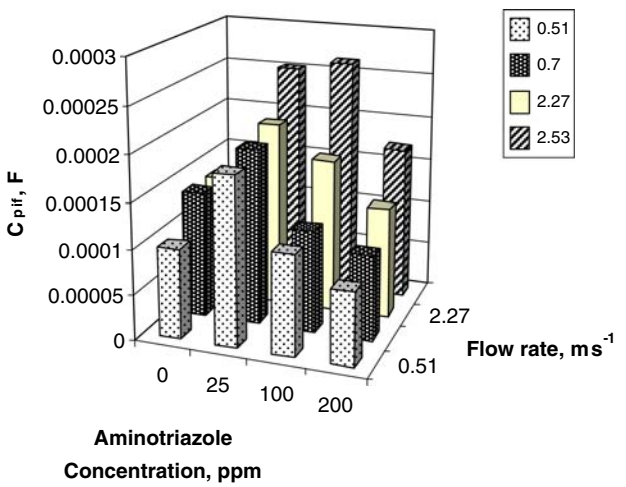

Fig. 13 Capacitance of porous inhibitor film as a function of aminotriazole concentration and flow rates

4 Conclusions

- The compact design of the flow loop constructed in this study can easily and economically be used in the evaluation of inhibitor performance, and its electrochemical behaviour in turbulent flow conditions.
- The aminotriazole inhibitor has some inhibitive effects in CO_2 corrosion of steel which may be due to adsorption and formation of a protective inhibitor film.
- There is a clear flow dependency of the electrochemical process taking place on the surface of the steel electrode.
- The flow dependency of the electrochemical process is detected by means of the variation with the flow-rate in the loop of the measured corrosion rate (expressed in terms of R_{ct}^{-1}) and the resistance and capacitance of the inhibitor film, R_{pif} and C_{pif}.
- The results obtained in this study indicate that the inhibitor concentration is not the sole factor to be considered in the qualification of the performance of a corrosion inhibitor. This is due to the fact that flow can also have a major effect upon the electrochemical corrosion process.
- Corrosion potential analysis suggest that the most likely way to decrease the corrosion rates is the effect of blocking the active sites on the metal surface by adsorbed aminotriazole molecules.
- With the increase of the inhibitor concentration, the inhibitor film capacitance decreases, while the pore solution resistance increases.
- The analysis shows that the formation of a very dense inhibitor film on the metal surface, rather than an increment of film thickness, could be used to explain both the decrease of charge-transfer resistance and the decrease of film capacitance.
- The information of charge-transfer resistance from EIS tests provides a very useful way to study performance of inhibitors. Other information such as film and double-layer capacitance can be used to characterize the mechanism of the inhibitor film.

Acknowledgments During this study, A. Garnica-Rodriguez was supported by a MSc scholarship from CONACYT (Mexico). The authors would like to thank the Laboratory of Corrosion of The Directorate of Exploration and Production of the Mexican Petroleum Institute (IMP) for the facilities provided for the development of this study.

References

1. Sastri VS (1998) Corrosion inhibitors. Wiley, New York
2. Newton LE, Hausler RH (eds) (1984) Carbon dioxide corrosion in oil and gas production—selected papers, abstracts and references. Compiled reference book. National Association of Corrosion Engineers (NACE), T-1-3, Houston

3. Goddard H (ed) (1984/1985) Advances in CO_2 corrosion, vols 1, 2. National Association of Corrosion Engineers (NACE), Houston
4. Rothmann B, Schmitt G (1978) Werkst Korros 29:237
5. Cao C (1996) Corros Sci 38:2073
6. Wang D, Li S, Ying Y, Wang M, Xiao H, Chen Z (1999) Corros Sci 41:1911
7. Hackerman N, Hurd RM (1962) Proceedings of the international conference on metallic corrosion. Butterworths, London, pp 166
8. Wang HB, Shi H, Hong T, Kang C, Jepson WP (2001) Paper # 01023, Corrosion'01. NACE International, Houston
9. Crolet J, Thevenot N, Nesic S (1996) Paper # 04, Corrosion'96. NACE International, Houston
10. Schmitt G, Mueller M, Papenfuss M, Strobel-Effertz E (1999) Paper # 038, Corrosion'99. NACE International, Houston
11. Beaunier L, Epelboin I, Lestrade JC, Takenouti H (1976) Surf Technol 4:237
12. Mansfeld F, Tsai CH (1991) Corrosion 47:958
13. Thompson I, Campbell D (1994) Corros Sci 36:187
14. Videm K, Kvarekvaal J, Perez T, Fitzsimons G (1996) Paper # 001, Corrosion'96. NACE International, Houston
15. Grimm RD, Landolt D (1994) Corros Sci 36:1847
16. Silverman DC Tutorial on CYLEXPERT^{TM} and the rotating cylinder electrode. www.argentumsolutions.com
17. Mansfeld F, Kendig MW, Lorenz WJ (1985) J Electrochem Soc 132:290
18. Tan YJ, Bailey S, Kinsella B (1996) Corros Sci 38:1545
19. Walter GW (1986) Corros Sci 26:681
20. Mertens SF, Cooman BC, Temmerman E (1999) Corrosion 55:151
21. Kowata K, Takahashi K (1996) Paper # 219, Corrosion'96. NACE International, Houston